GATE simulation based feasibility studies of in-beam PET monitoring in ^{12}C beam cancer therapy

WU Jing LIU Yaqiang MA Tianyu* WEI Qingyang WANG Shi CHENG Jianping

Key Laboratory of Particle & Radiation Imaging, Ministry of Education,

Department of Engineering Physics, Tsinghua University, Beijing 100084, China

Abstract In comparison with conventional radiotherapy techniques, ^{12}C beam therapy has its significant advantage in cancer treatment because the radiation dose are mostly concentrated near the Bragg peak region and damage to normal tissues along the beam path is thus greatly reduced. In-beam PET provides a way to monitor dose distribution inside human body since several kinds of positron-emitting nuclei are produced through the interaction between ^{12}C beam and body matters. In this work, we study the quantitative relationship between the spatial location of the Bragg peak and the spatial distribution of positrons produced by positron-emitting nuclei. Monte Carlo package GATE is used to simulate the interactions between the incident ^{12}C beam of different energies (337.5, 270.0 and 195.0 MeV/u) and various target matters (water, muscle and spine bone). Several data post-processing operations are performed on the simulated positron-emitting nuclei distribution data to mimic the impacts of positron generation and finite spatial resolution of a typical PET imaging system. Simulation results are compared to published experimental data for verification. In all the simulation cases, we find that ^{10}C and ^{11}C are two dominant positron-emitting nuclei, and there exists a significant correlation between the spatial distributions of deposited energy and positrons. Therefore, we conclude that it is possible to determine the location of Bragg peak with 1 mm accuracy using current PET imaging systems by detecting the falling edge of the positron distribution map in depth direction.

Key words Monte Carlo simulation, Heavy-ion therapy, Positron emission tomography (PET), In-beam monitoring, Bragg peak

1 Introduction

Particle therapy (PT) has been used as a powerful tool in cancer treatment [1]. When an energetic particle beam travels through a target matter, the energy deposition curve has a pronounced Bragg peak, where most of the particle beam energy is deposited. This is a unique merit of particle therapy over conventional radiotherapy approaches, for that a higher dose can be delivered within the target tumor region and a lower dose is deposited in the normal tissues. Among the types of particles for PT, i.e. proton[2], ^{3}He[3], and ^{12}C [4], ^{12}C beam, which is termed as heavy ion, has the narrowest Bragg peak, and the highest energy loss portion near the Bragg peak. These lead to a larger peak-to-plateau ratio and therefore a better relative biological effectiveness (RBE) in the tumor[4, 5].

During the process of heavy-ion therapy, several kinds of positron-emitting nuclei are produced by the nuclear interaction between the incident ions and the target nuclei. Recent research interests are focused on this effect because it enables in-beam monitoring of the location and intensity of the incident

This work was supported in part by Specialized Research Fund for the Doctoral Program of Higher Education (SRFDP200800031071), National Natural Science Foundation of China (No. 10975086), and the National High Technology Research and Development Program (“863” Program) of China (No. 2006AA020802).

* Corresponding author. *E-mail address:* maty@tsinghua.edu.cn

Received date: 2010-08-06

heavy-ion beams by using the imaging technique of positron emission tomography (PET), which provides accurate information of positron distribution by detecting annihilated photon pairs from electron-positron annihilation and reconstructing the spatial distribution map of the positrons. Recently, Geant4[6] based Monte Carlo simulation studies[7, 8] and experimental studies[9] of in-beam PET monitoring in heavy-ion therapy have been performed to study the spatial relationship between deposited energy and positrons. The studies indicated that the positron distribution produced by ^{12}C beam is suitable for PET monitoring, as there is also a peak on the positron distribution curve. However, the exact relationship of spatial distributions between the positron peak and Bragg peak shall be investigated quantitatively, so as to be of help in predicting the actual location of the Bragg peak from the PET image.

For simulation of such a process, the Monte-Carlo package dedicated to emission tomography simulation, GATE (Geant4 Application for Tomographic Emission) [10] is advantageous over the Geant4 package used in Refs.[7] and [8], because specific tools were added in its latest version, GATE v6.0.0, for radiation therapy applications, and modeling and simulation of PET imaging process with a typical PET system is much easier. In this work, interactions between ^{12}C beam and various target matters were simulated with GATE and the quantitative relationship of spatial distributions between the Bragg peak and the positron peak was studied.

2 Methods

2.1 Physical model of ^{12}C beam interaction with matters in GATE

There are two kinds of physical reaction processes between the ^{12}C beam and target matter: electromagnetic processes and hadronic processes. Both processes are modeled in the simulation.

In the electromagnetic processes [6, 7, 8, 10], ionization is the major cause of energy deposition, which was calculated using the Bethe-Bloch formula [11, 12]. Other electromagnetic processes include photoelectron emission, Compton scattering, pair production, bremsstrahlung and electron-positron annihilation. Multiple scattering is also introduced for charged particles that exist in the interaction process.

The hadronic processes[6, 10] include elastic scattering and inelastic processes. The positron-emitting nuclei are produced in the inelastic processes of three main steps: cascade, pre-equilibrium and de-excitation. In the GATE simulation, we used the binary cascade model, which terminates when the average and maximum energy of secondary particles are below the specified threshold. Appropriate pre-compound and de-excitation models were included in the simulation to treat the remaining fragments after the cascade step.

2.2 Simulation setup

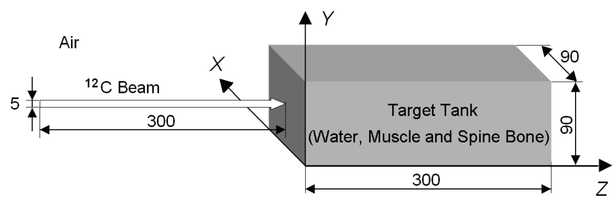

Fig. 1 The diagram of the simulation geometry in GATE.

Fig. 1 shows geometry for the GATE simulation. The target tank of 90 mm × 90 mm × 300 mm was filled with homogeneous materials of H_2O (ρ = 1.00 g/cm^3), muscle (ρ = 1.05 g/cm^3) and spine bone (ρ = 1. 42 g/cm^3). The muscle consisted of H(10.20%), C(14.30%), N(3.40%), O(71.00%), Na(0.10%), P(0.20%), S(0.30%), Cl(0.10%) and K(0.40%), while the spine bone consisted of H(6.30%), C(26.10%), N(3.90%), O(43.60%), Na(0.10%), Mg(0.10%), P(6.10%), S(0.30%), Cl(0.10%), K(0.10%) and Ca(13.30%). In the simulation, we used ^{12}C ion beams of 337.5, 270.0 and 195.0 MeV/u, with a Φ5 mm beam spot, coming out of the vacuum window placed at 300 mm from the tank, in perpendicular incidence (Z axis) to the tank surface. We note that choice of this distance has a significant influence on the simulation result, because the attenuation of ^{12}C beam in air cannot be ignored. With the same energy, the closer the beam source is towards the target tank, the deeper the locations of Bragg peak and positron peak are. The ^{12}C beams' attenuation in air was simulated with the following parameters: ρ = 1.29 mg/cm^3, composition:

N(75.53%), O(23.18%), Ar(1.28%) and C(0.01%).

The GATE simulation was run on a 10-node Intel Xeon E5520 cluster. With the initial particles of 9×10^6 ^{12}C ions, the simulation ran for 20 hours.

2.3 Analytical modeling of positron decay

In clinical practice, the ^{12}C beam usually has a particular time structure. We set the simulation time to be 0.1 s in GATE simulation so that decay of the positron-emitting nuclei produced by GATE simulation can be ignored. Based on GATE simulation results of the positron-emitting nuclei distributions, we applied the same time structure of ^{12}C beam as used in Ref. [8, 9] to model the positron decay process. Therefore, we could compare our simulation results with the literature data. This step was performed on the simulated data with a Matlab program.

The time structure of ^{12}C beam has K repeated particle spills of t_s with pauses of t_p between subsequent spills. In order to reduce the random coincidences, the PET detections are performed during beam pauses [8, 9]. We use $T_j = (t_p + t_s)\,(j–1) + t_s$ (j =1, …, K) to denote the end of j^{th} spill. Then the amount of the i^{th} positron-emitting nuclide N_i, which is a function of 3D space coordinates (x, y, z), is given by [8]:

$$\begin{aligned} \frac{\mathrm{d}N_i}{\mathrm{d}t} &= -\lambda_i N_i + Jn_i \quad (T_j - t_s \le t < T_j) \\ \frac{\mathrm{d}N_i}{\mathrm{d}t} &= -\lambda_i N_i \qquad\quad (T_j \le t < T_j + t_p) \end{aligned} \tag{1}$$

where n_i (in count/per particle), resulting from above GATE simulation, is the production rate of the i^{th} positron-emitting nuclide at coordinates (x, y, z) during the spill periods. J is the ^{12}C beam intensity (in count/s), and λ_i is the decay constant of the i^{th} positron-emitting nuclide.

Similar to the derivations in Ref. [8] and [13], the amount of the i^{th} positron-emitting nuclide at (x, y, z) at the end of j^{th} spill $N_{i,j}$ can be expressed recursively:

$$N_{i,j} = N_{i,j-1}\exp\left[-\lambda_i(t_s+t_p)\right] + \frac{Jn_i}{\lambda_i}\left[1-\exp(-\lambda_i t_s)\right], \quad (j=1,\cdots,K) \tag{2}$$

where $N_{i,0} = 0$. Therefore, the total number of positrons emitted by all the positron-emitting nuclei at coordinates (x, y, z) during all the beam pauses is

$$\begin{aligned} N &= \sum_i \sum_{j=1}^{K-1} N_{i,j}(1-\exp(-\lambda_i t_p)) \\ &= \sum_i \{\left[1-\exp(-\lambda_i t_p)\right] \times \\ &\sum_{j=1}^{K-1}[\frac{Jn_i}{\lambda_i}(1-\exp(-\lambda_i t_s))\sum_{m=0}^{j-1}\exp(-\lambda_i(t_s+t_p)m)]\} \end{aligned} \tag{3}$$

where m is a loop index.

In our study, the parameters chosen are the same as in Ref. [8, 9] for ^{12}C beam: $J = 0.9\times10^8$ counts/s, K=120, t_s=2.2s and t_p=2.29s.

2.4 Approximate modeling of PET imaging process

Practical PET systems have limited spatial resolution, which means the reconstructed PET image can be considered as only a "blurred" version from the original positron spatial distribution. This effect is taken into account through a further data post-processing step. For a typical PET system, the system resolution R_{sys} depends on several factors [14], which can be estimated by:

$$R_{sys} \approx \sqrt{R_d^2 + R_r^2 + R_{nc}^2} \tag{4}$$

where, R_d=4mm is the intrinsic geometrical resolution of the detector; R_r is the effective positron range before annihilation, and R_{nc} is the contribution of non-colinearity of annihilated photon pairs to the spatial resolution. Since in this simulation the most abundant positron-emitting nuclide is ^{11}C, we chose R_r=0.39 mm, which corresponds to the root mean square effective range for positrons emitted by ^{11}C [15]. R_{nc} can be determined by R_{nc} = 0.0022 D, where D is diameter of the detector ring. In this work a typical value of D = 800 mm was selected.

The system resolution calculated from Eq. (4) is 4.39 mm. In order to further accommodate the impacts of other long-positron-range nuclides and variation of PET system setup, a slightly larger R_{sys} (5 mm) was used in following studies.

With the 3D spatial distribution map of positrons calculated by the method described in Section 2.3, the spatial distribution of positrons along Z direction could be obtained by data summation over the *X*-*Y* plane. Then it was convolved with a 1-D Gaussian kernel (FWHM= 5 mm) through *Z* direction. The resultant positron distribution map was compared to that of the deposited energy which was obtained from GATE simulation.

3 Results

3.1 Spatial distributions of deposited energy and positron-emitting nuclei based on GATE

Curves of deposited energy and spatial distribution of positron-emitting nuclei after summation over *X*-*Y* plane as functions of Z are shown in Fig. 2. The ^{12}C beam energy was 337.5 MeV/u and the target tank was filled with water. It can be seen that when the ^{12}C beam traveled 300 mm in air to the tank surface, the Bragg peak was at 206 mm depth. The ^{12}C beam interacts with the target matter and produces the positron-emitting nuclei of ^{11}C, ^{10}C, ^{13}N, ^{14}O, ^{15}O and ^{17}F. The ^{11}C and ^{10}C are mainly produced by removing one and two neutrons, respectively, from the incident ^{12}C nuclide, there exist certain peaks on their spatial distribution curves. One can notice a strong correlation of the spatial location between these peaks and the Bragg peak, and especially the falling edge of the ^{11}C peak almost overlaps with that of the Bragg peak. The fragments ^{13}N, ^{14}O and ^{15}O produced by target matter are almost uniformly distributed due to little momentum transfer in nuclear reactions between the incident particles and the target nuclei. However, their contributions to the peak position are much less than the ^{11}C peak.

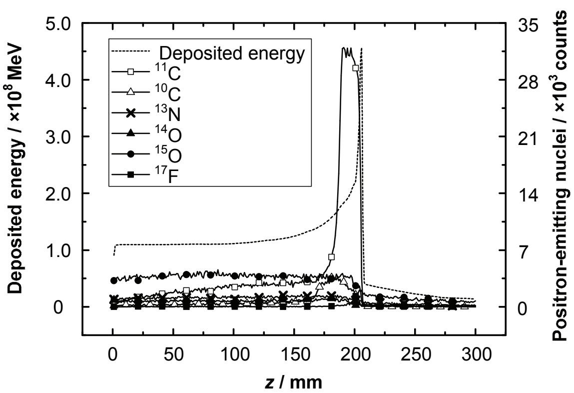

Fig. 2 Distributions of deposited energy and positron-emitting nuclei as functions of *z* (^{12}C beam energy: 337.5 MeV/u, target matter: water).

3.2 Spatial distribution of positrons

Fig. 3 shows 2D profiles of the 3D distributions of deposited energy and positrons obtained by method described in Section 2.3. Similar to the spatial distribution of ^{11}C nuclide, the positrons are significantly concentrated over the end of the incident beam.

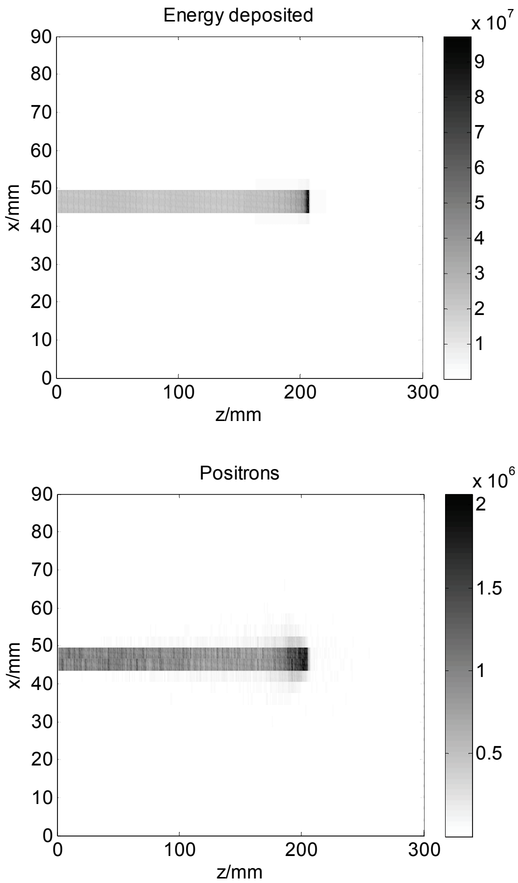

Fig. 3 The horizontal profiles of deposited energy and positrons (^{12}C beam energy: 337.5 MeV/u, target matter: water).

As is described in Section 2.4, the distributions of deposited energy and positrons for 337.5 MeV/u ^{12}C beam in water as functions of *Z* are shown in Fig. 4. The in-beam PET experimental data from Refs. [8] and [9] were plotted in hollow dots for comparison. The black solid curve presents the simulation results of positron distribution, which agree well with the experimental data in most of the regions. The exceptions are the tails, but the difference in the tails has little influence on this study, which is aimed at comparing the spatial relationship between the peaks.

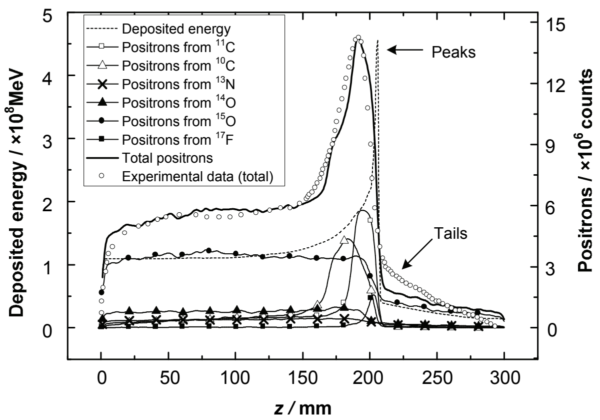

Fig. 4 Distributions of deposited energy and positrons as functions of z (^{12}C beam energy: 337.5 MeV/u, target matter: water). The in-beam PET experimental positron data taken from Ref. [8, 9] are plotted by hollow dots for comparison.

Similar to the results in Fig. 2, there is also a pronounced peak on the positron distribution curve which aligns with the Bragg peak on the energy deposition curve very well. Therefore, once we quantify the spatial relationship between them, the location of Bragg peak can be very accurately estimated by the positron distribution map measured from in-beam PET imaging.

3.3 Quantification of the spatial relationship of peak locations

As Fig. 4 shows, a definite spatial relation may exist between the Bragg peak and the positron peak. Differences in the peak positions and the falling edge positions can be calculated for comparison. A series of simulations were performed with combinations of different ^{12}C beam energies (337.5, 270.0 and 195.0 MeV/u) and different target matters (water, muscle and spine bone). Simulated data were post-processed as described in Section 2.3 and 2.4. The spatial distributions of deposited energy and positrons are shown in Fig. 5.

From the data in Fig.5, the peak positions of both curves were determined by the positions of their maximum values, and the relative distances between the peak positions were calculated, while the falling edge positions of both curves were calculated according to the positions of the fastest gradient descent on the curves. Relative distances between the falling edges were also calculated and listed in Table 1.

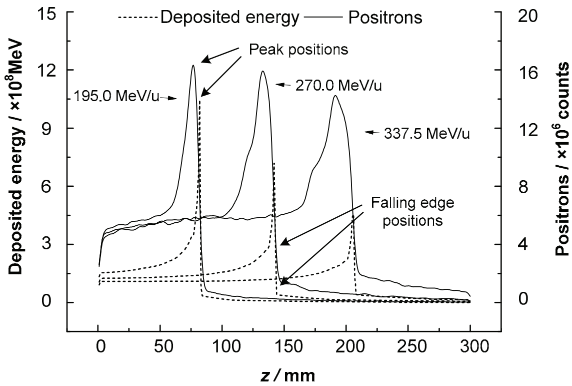

(a)

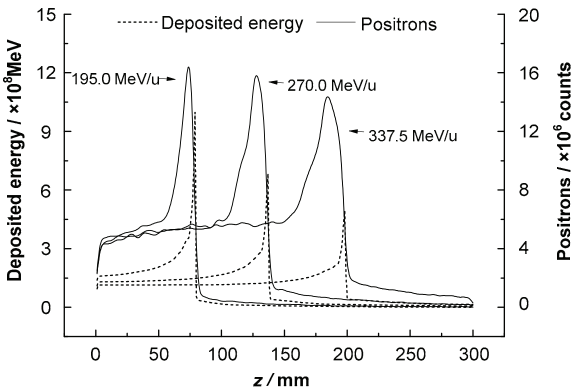

(b)

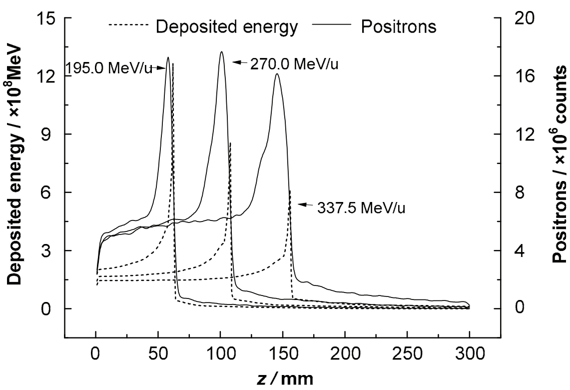

(c)

Fig.5 Spatial distributions of positrons and deposited energy as functions of z for ^{12}C beam (a) in water; (b) in muscle; (c) in spine bone. Energies of ^{12}C beam are 337.5, 270.0 and 195.0 MeV/u.

Table 1 Spatial relationship between the Bragg peak and the positron peak.

Target matter	Beam energy / MeV/u	Peak position / mm			Falling edge position / mm		
		Bragg peak	Positron peak	Relative distance	Bragg peak	Positron peak	Relative distance
Water	337.5	206.0	191.5	14.5	206.0	205.0	1.0
	270.0	142.0	133.0	9.0	142.0	141.0	1.0
	195.0	82.0	77.0	5.0	82.0	81.0	1.0
Muscle	337.5	198.0	184.5	13.5	198.0	197.0	1.0
	270.0	137.0	128.0	9.0	137.0	136.0	1.0
	195.0	79.0	74.0	5.0	79.0	78.0	1.0
Spine bone	337.5	156.0	145.5	10.5	156.0	155.0	1.0
	270.0	108.0	101.0	7.0	108.0	107.0	1.0
	195.0	62.0	58.0	4.0	62.0	61.5	0.5

The results in Table 1 indicate that it may not be a wise choice to use the relative distance between the peak positions of both curves to describe the spatial relationship between the Bragg peak and the positron peak, because it varies with the beam energy and the target material. However, in all cases, the relative distance between the falling edge positions of both curves is within 1 mm. As shown in Table 1, the peak position and the falling edge position of the Bragg peak are exactly the same. Therefore, one can mark the actual position of the Bragg peak with 1 mm accuracy by detecting the falling edge of the positron distribution curve with in-beam PET.

4 Conclusion

In this work, we studied the feasibility of using in-beam PET to monitor ^{12}C beam distribution in heavy-ion therapy. We used GATE to simulate ^{12}C beam with different beam energies and in different target matters. The simulated data were post-processed to model the effects of radio-nuclide decay and spatial resolution degradation of in-beam PET system. Results show that in all simulated cases, there exists clear spatial relationship between the distributions of deposited energy and positrons. Therefore, by detecting the falling edge of the positron distribution map in depth direction, it is possible to locate the Bragg peak with 1 mm accuracy with current PET technique. Introduction of in-beam PET in clinical cancer therapy practice may bring great benefit for improving the positioning accuracy of current heavy-ion cancer therapy systems. In future work, we will simulate the in-beam PET detection process and investigate the application of depth-of-interaction (DOI)[16] and accurate system modeling[17] techniques to improve the accuracy of PET reconstruction images.

References

1 Jäkel O, Schulz-Ertner D, Karger C P, *et al*. Technol. Cancer Res Treat, 2003, **2**: 377–387.

2 Olsen D R, Bruland Øyvind S, Frykholm G, *et al*. Radiother. Oncol., 2007, **83**: 123–132.

3 Char D H, Kroll S M., Castro J. Am J Ophthalmol, 1998, **125**: 81–89.

4 Tsujii H, Mizoe J, Kamada T, *et al*. Radiother Oncol, 2004, **73**: 41–49.

5 Tsujii H, Kamada T, Baba M, *et al*. New J. Phys., 2008, **10**: 075009 (16pp).

6 Agostinelli S, Allison J, Amako K, *et al*. Nucl. Instrum. Methods, 2003, **506**: 250–303.

7 Pshenichno I, Mishustin I, Greiner W. Phys. Med. Biol., 2005, **50**: 5493–5507.

8 Pshenichnov I, Larionov A, Mishustin I, *et al*. Phys. Med. Biol., 2007, **52**: 7295–7312.

9 Fiedler F, Crespo P, Parodi K, *et al*. IEEE Trans. Nucl. Sci., 2006, 53: 2252–2259.

10 Jan S, Santin G, Strul D, *et al*. Phys. Med. Biol., 2004, **49**: 4543–4561.

11 Yao W M., Amsler C, Asner D, *et al*. J. Phys. G: Nucl. Part. Phys., 2006, **33**: 252–296.

12 Ahlen S P. Rev Mod Phys, 1980, **52**: 121–173.

13 Parodi K, Enghardt W, Haberer T. Phys Med Biol, 2002, **47**: 21–36.

14 Cherry S R, Sorenson J A, Phelps M E. Physics in Nuclear Medicine. Pennsylvania: W.B. Saunders, 2003, 328–333.

15 Derenzo S E. IEEE Trans. Nucl Sci, 1986, **33**: 565–569.

16 Shao Y, Yao R, Ma T. Med Phys, 2008, **35**:5829-5840.

17 Yao R, Ma T, Shao Y. IEEE Trans. Nucl. Sci., 2009, **56**: 2651-2658.